ADVANCED MATERIALS

Supporting Information

for *Adv. Mater.,* DOI: 10.1002/adma.202102967

Miniaturized VIS-NIR Spectrometers Based on Narrowband and Tunable Transmission Cavity Organic Photodetectors with Ultrahigh Specific Detectivity above 10^{14} Jones

Shen Xing, Vasileios Christos Nikolis, Jonas Kublitski, Erjuan Guo, Xiangkun Jia, Yazhong Wang, Donato Spoltore, Koen Vandewal, Hans Kleemann, Johannes Benduhn,* and Karl Leo**

Supporting Information

Miniaturized VIS-NIR Spectrometers based on Narrowband and Tunable Transmission Cavity Organic Photodetectors with Ultrahigh Specific Detectivity above 10^{14} Jones

Shen Xing, Vasileios Christos Nikolis, Jonas Kublitski, Erjuan Guo, Xiangkun Jia, Yazhong Wang, Donato Spoltore, Koen Vandewal, Hans Kleemann, Johannes Benduhn* and Karl Leo**

Supporting Figures

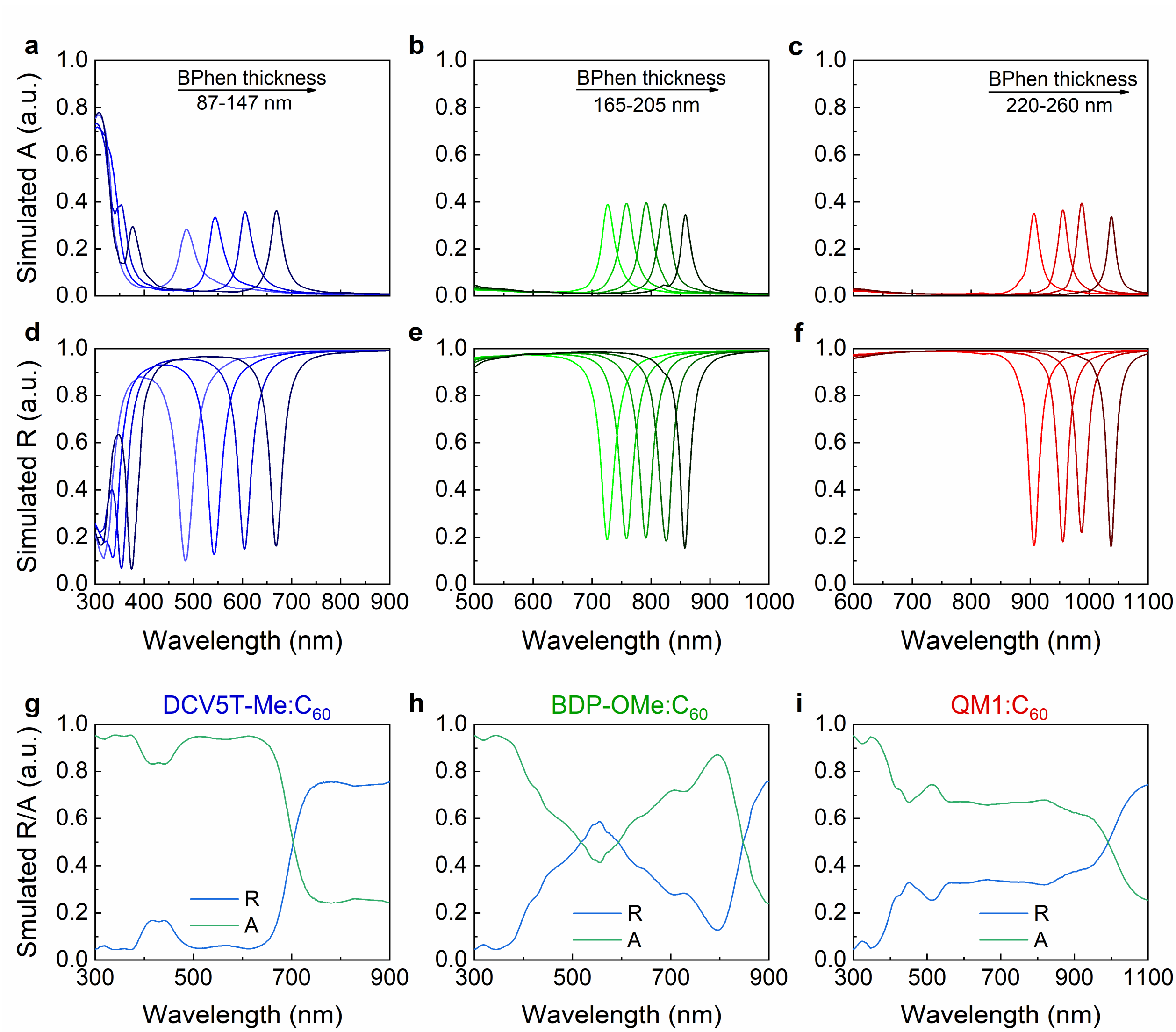

Figure S1. Simulated absorption (A) and reflection (R) spectra of TCs and OPDs. Simulated A and R spectra of (**a-f**) TCs and (**g-i**) OPDs based on different active blends as labeled above each subfigure.

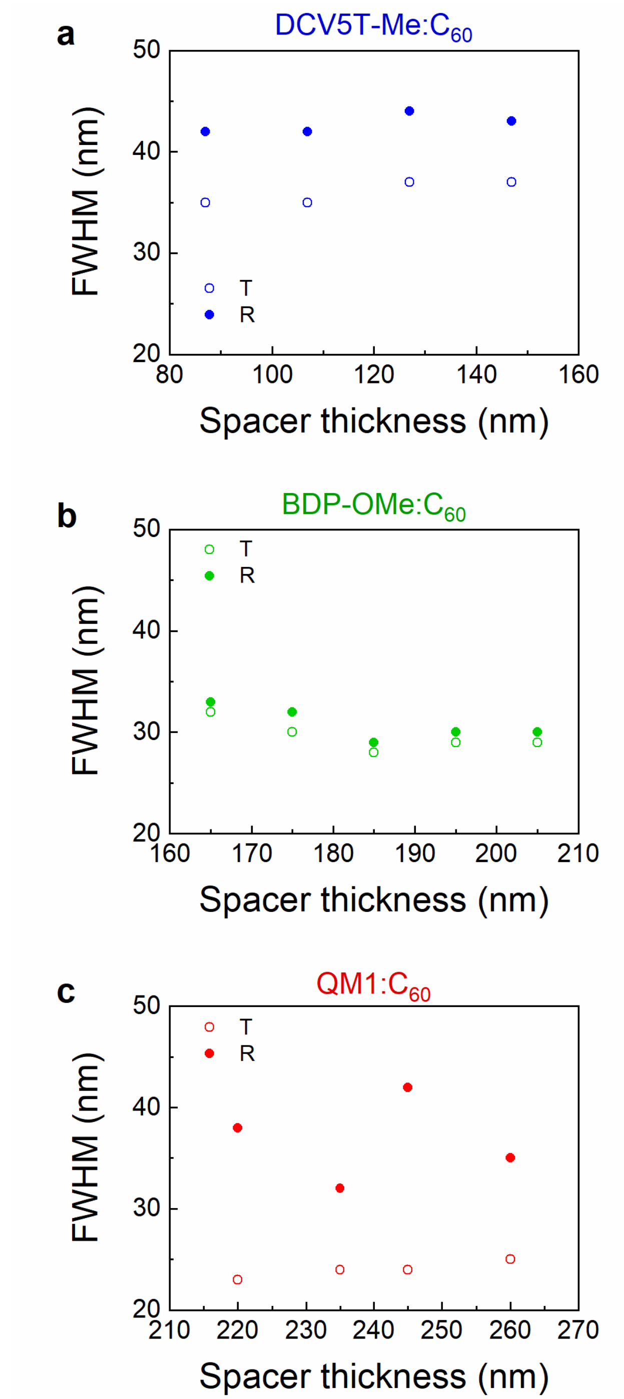

Figure S2. Spectral resolution of TC-OPDs. Comparison of the FWHM of the responsivity peak (*R*) of TC-OPDs and transmission (*T*) of TC based on different active blends (**a**) DCV5T-Me:C_{60}, (**b**) BDP-OMe:C_{60}, and (**c**) QM1:C_{60}, respectively. All devices show a narrow FWHM down to ~40 nm.

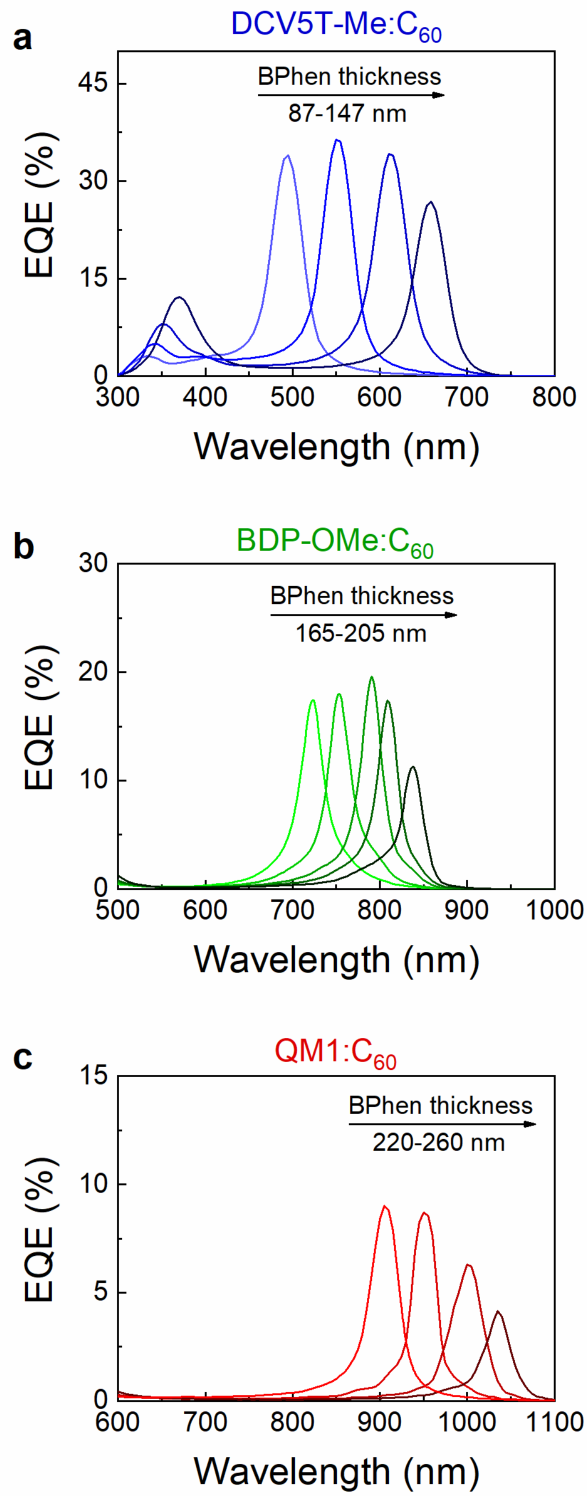

Figure S3. EQE spectra of TC-OPDs. EQE spectra of TC-OPDs for varied spacer (BPhen) layer thicknesses at zero bias based on different active blends (**a**) DCV5T-Me:C_{60}, (**b**) BDP-OMe:C_{60}, and (**c**) QM1:C_{60}, respectively.

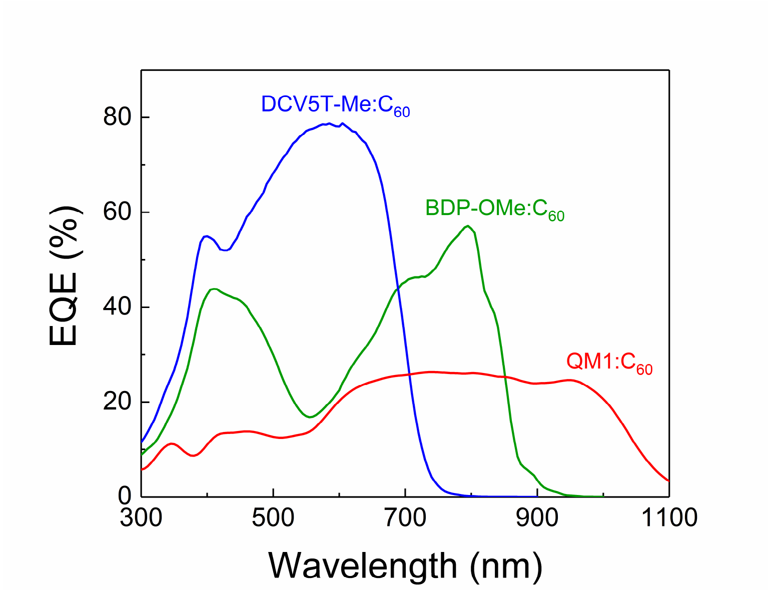

Figure S4. EQE spectra of the three OPDs without TC structure.

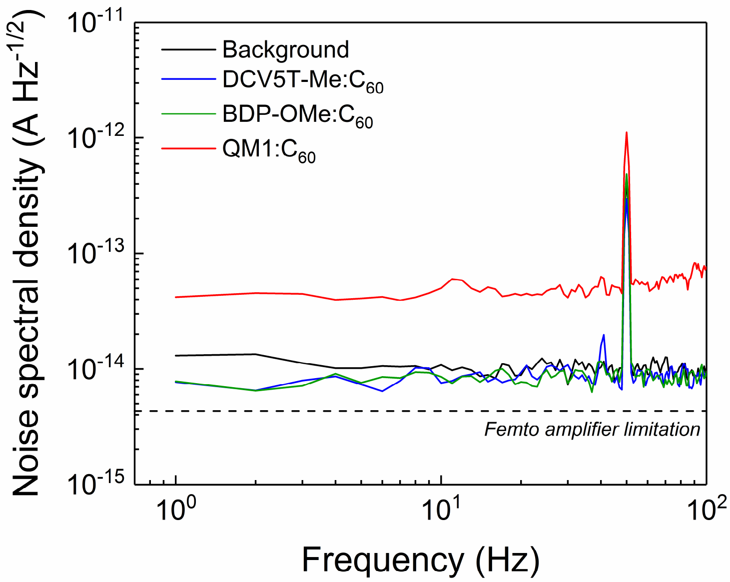

Figure S5. Noise spectral density of TC-OPDs. The spectra are calculated from Welch's method of the time-dependent dark current at zero bias of TC-OPDs based on different active blends. The current Femto preamplifier we use sets a limitation of 4.3 fA Hz$^{-1/2}$ as specified with the black dashed line. Our setup limitation is around 9 fA Hz$^{-1/2}$, being significantly larger than the thermal noise spectral density of TC-OPDs based on active blends DCV5T-Me:C_{60} and BDP-OMe:C_{60}. For these devices, the measured background noise of our setup overlaps with the measured signal, indicating that the real noise level is beyond the sensitivity of our setup.

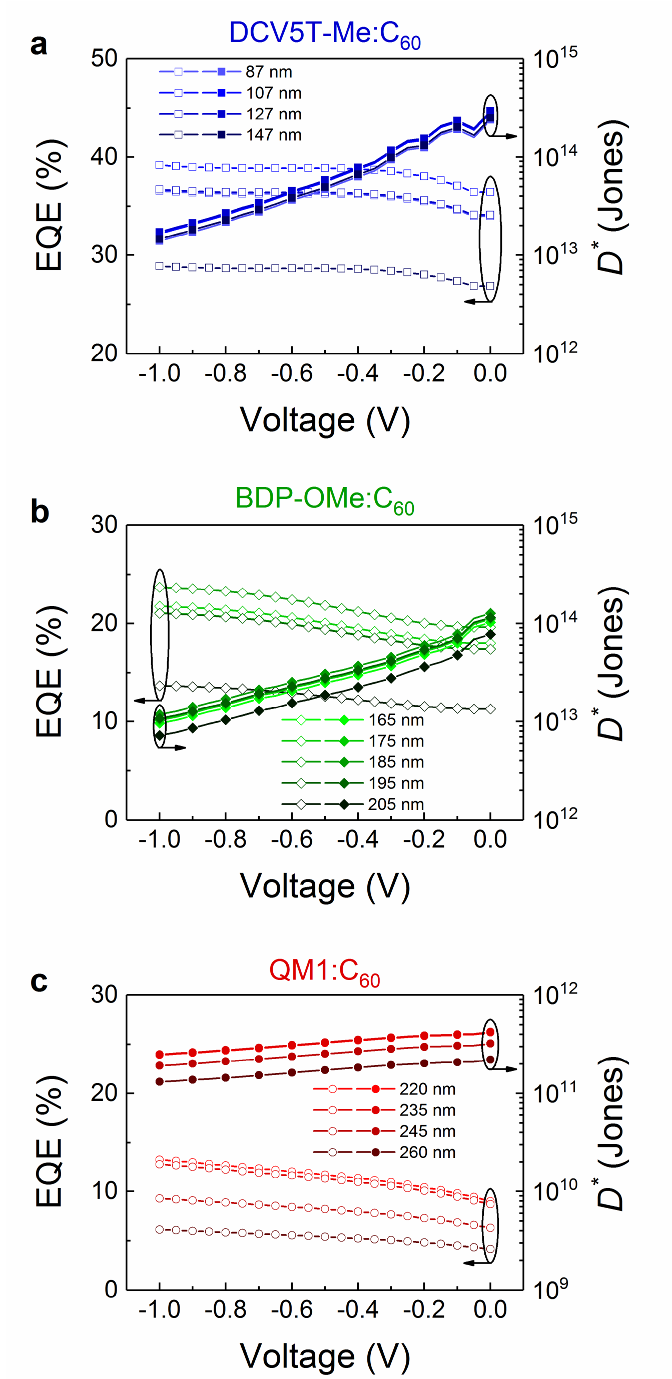

Figure S6. EQE and D^* of TC-OPDs at peak wavelength as a function of applied voltage. EQE and D^* of TC-OPDs with varied spacer (BPhen) layer thicknesses as a function of applied reverse bias based on different active blends (**a**) DCV5T-Me:C_{60}, (**b**) BDP-OMe:C_{60}, and (**c**) QM1:C_{60}. The specific detectivities in (**a**) and (**b**) are obtained from the calculated sum of thermal and shot noise spectral density ($S_n = S_{thermal} + S_{shot} = (4k_BT/R_{sh} + 2qI_d)^{1/2}$). The D^* in (**c**) is acquired from the sum of measured thermal noise and calculated shot noise spectral density. Here, q is the elementary charge, and I_d represents the dark current at a reverse bias voltage.

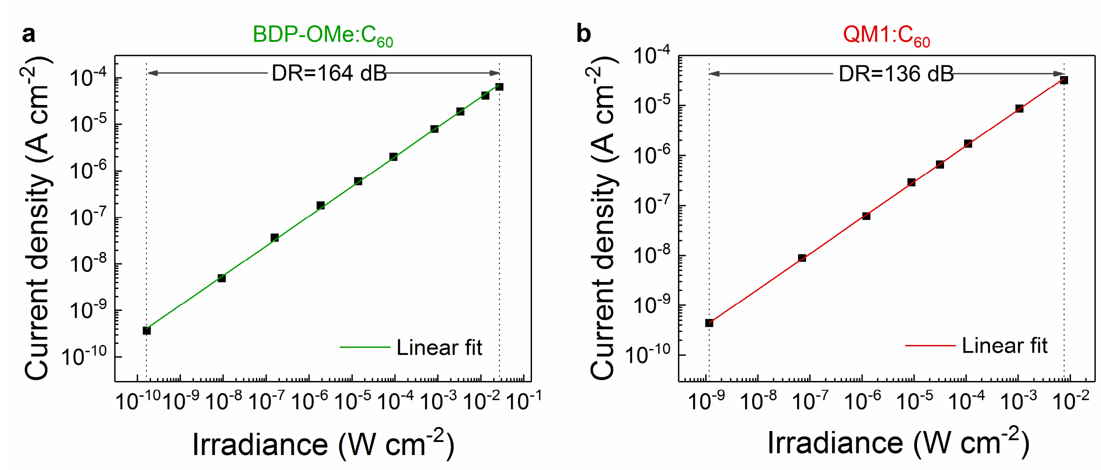

Figure S7. DR of TC-OPDs. Photoresponse of TC-OPDs for varying light intensity measured at zero bias based on active blends (**a**) BDP-OMe:C_{60} and (**b**) QM1:C_{60}.

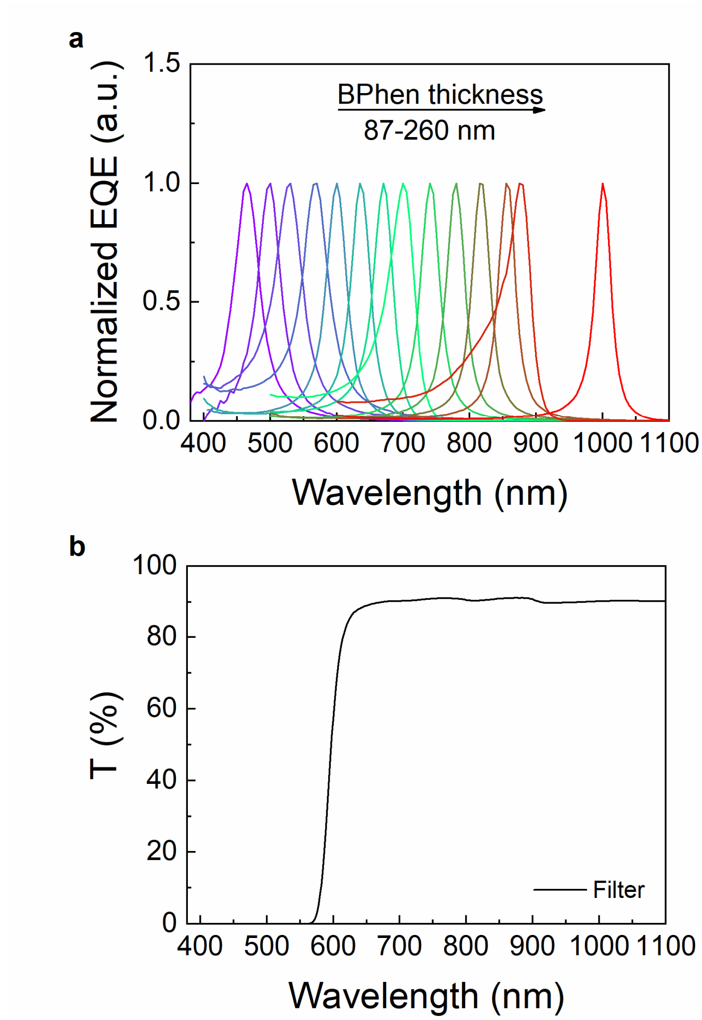

Figure S8. The EQE spectra of photodetecting pixels in a miniaturized spectrometer and longpass filter transmission. a Normalized EQE spectra of photodetecting pixels in a miniaturized spectrometer at zero bias with varied spacer (BPhen) layer thicknesses. The photoresponse peak is finely tuned from 465 to 1000 nm. **b** Transmission spectrum of the longpass filter. During the transmission measurement of the semi-transparent solar cell, short wavelengths (< 575 nm) are used to block the influence of the second resonance peak of BDP-OMe-based and QM1 based-TC-OPDs. The layer configuration of the semi-transparent solar cell is ITO (90 nm) / MH250:$W_2(hpp)_4$ (7 wt%, 5 nm) / C_{70} (15 nm) / BDP-OMe:C_{60} (1:2 substrate temperature at 100 °C during film deposition, 40 nm) / BF-DPB (5 nm) / BPAPF:NDP9 (10 wt%, 40 nm) / NDP9 (1 nm) / MoO_3 (3 nm) / Au (1 nm) / Ag (7 nm).

Supporting Tables

Table S1. Device stacks of all investigated TC-OPDs. For the devices, the following materials are used: the electrode materials: ITO (Thin Film Devices, USA) and Al (Kurt J. Lesker), the donor materials: DCV5T-Me (Synthon, Germany), BDP-OMe (TU Dresden, Germany), and QM1 (TU Dresden, Germany), the acceptor material: C_{60} (Lumtec, Taiwan), the transport layer materials: BPAPF (Lumtec, Taiwan), BF-DPB (Synthon, Germany) and HATNA-Cl_6 (Lumtec, Taiwan), the dopants: F_6-TCNNQ (Novaled GmbH, Germany) and $W_2(hpp)_4$ (Novaled GmbH, Germany), the spacer material: BPhen (Lumtec, Taiwan), the seed layer materials: MoO_3 (Sigma-Aldrich, USA) and Au (Allgemeine Gold und Silberscheidanstalt, Germany) and the mirror material: Ag (Kurt J. Lesker).

Active blend	**Stack**
DCV5T-Me:C_{60}	Ag (30 nm) / BPhen (varied thicknesses) / Ag (30 nm) / Au (1 nm) / MoO_3 (3 nm) / Glass (1 mm) / ITO (90 nm) / BPAPF:F_6-TCNNQ (3 wt%, 40 nm) / BPAPF (5 nm) / DCV5T-Me:C_{60} (2:1, 40 nm) / C_{60} (15 nm) / HATNA-Cl_6 (10 nm) / HATNA-Cl_6:$W_2(hpp)_4$ (3 wt%, 10 nm) / Al (100 nm)
BDP-OMe:C_{60}	Ag (30 nm) / BPhen (varied thicknesses) / Ag (30 nm) / Au (1 nm) / MoO_3 (3 nm) / Glass (1 mm) / ITO (90 nm) / BPAPF:F_6-TCNNQ (3 wt%, 40 nm) / BPAPF (5 nm) / BDP-OMe:C_{60} (1:2 substrate temperature at 90 °C, 50 nm) / C_{60} (15 nm) / HATNA-Cl_6 (10 nm) / HATNA-Cl_6:$W_2(hpp)_4$ (3 wt%, 10 nm) / Al (100 nm)
QM1:C_{60}	Ag (30 nm) / BPhen (varied thicknesses) / Ag (30 nm) / Au (1 nm) / MoO_3 (3 nm) / Glass (1 mm) / ITO (90 nm) / BF-DPB:F_6-TCNNQ (5 wt%, 25 nm) / BF-DPB (5 nm) / QM1:C_{60} (1:2, 50 nm) / C_{60} (15 nm) / HATNA-Cl_6 (10 nm) / HATNA-Cl_6:$W_2(hpp)_4$ (3 wt%, 10 nm) / Al (100 nm)

Table S2. Key parameters of TC-OPDs. Response peak, responsivity (R), on-off ratio at 100 mW cm^{-2} illumination, specific detectivity (D^*), shunt resistance (R_{sh}), and noise current at zero bias.

Active blend	**Response peak (nm)**	R **(A W^{-1})**	**On-off ratio (×10^8)**	D^* **(×10^{14} Jones)**	R_{sh} **(×10^9 Ω)**	**Noise current (fA Hz$^{-1/2}$)**
DCV5T-Me:C_{60}	495	0.14	4.9	2.4	777	0.14
	550	0.16	6.0	2.8		
	615	0.17	6.6	3.0		
	660	0.14	5.6	2.5		

Active blend	**Response peak (nm)**	R **(A W^{-1})**	**On-off ratio (×10^8)**	D^* **(×10^{14} Jones)**	R_{sh} **(×10^9 Ω)**	**Noise current (fA Hz$^{-1/2}$)**
BDP-OMe:C_{60}	724	0.10	3.2	1.0	258	0.25
	754	0.11	3.4	1.1		
	790	0.12	3.6	1.3		
	810	0.11	3.4	1.1		
	840	0.08	3.0	0.8		

Active blend	**Response peak (nm)**	R **(A W^{-1})**	**On-off ratio (×10^7)**	D^* **(×10^{11} Jones)**	R_{sh} **(×10^6 Ω)**	**Noise current (fA Hz$^{-1/2}$)**
QM1:C_{60}	905	0.07	3.9	4.2	30	40
	950	0.07	2.9	4.2		
	1000	0.05	2.9	3.2		
	1035	0.03	2.6	2.2		

Table S3. Summary of previously reported photodetectors. Detailed information of previously reported organic, inorganic, and perovskite photodetectors shown in Figure 4d.

	Active material	Wavelength range (nm)	D^* (Jones)	Bias (V)	Comment	Ref.
Broadband	PBDTTT-EFT: eh-IDTBR	400-800	1.6×10^{13}@720 nm	-1.0	Non-Fullerene	[1]
	PBDTTT-C-T: FOIC	300-1000	2.0×10^{13}@820 nm	-1.0	Non-Fullerene/ Thick junction	[2]
	ClAlPc:C_{70}	300-800	4.0×10^{13}@730 nm	0.0	Small molecule	[3]
	PTB7-Th: CO_i8DFIC: $PC_{71}BM$	400-1000	8.0×10^{11}@670 nm	0.0	Non-Fullerene/ Ternary	[4]
	PTB7-Th: IFIC-i-4F: $PC_{71}BM$	300-1000	1.0×10^{14}@600 nm	0.0	Ternary	[5]
	PBDTTBTQ: $PC_{60}BM$	300-1100	3.0×10^{11}@1000 nm	-1.0		[6]
	PBDB-T: PNDI-FT10	400-800	2.0×10^{12}@600 nm	-3.0	All polymer	[7]
	Organic:PbS	400-1000	1.1×10^{13}@650 nm	40.0	Bilayer	[8]
	PBT:$PC_{61}BM$ PBTt:$PC_{61}BM$	300-1600	7.7×10^{10}@900 nm 2.5×10^{11}@900 nm	-0.1		[9]
	PbS:Perovskite	400-800	2.1×10^{13}@500 nm	-1.0	PM	[10]
	1-BF4:C_{60} 1-TPFB:C_{60} 2-BF4:C_{60}	400-1600	3.7×10^{9}@1000 nm 5.3×10^{10}@1000 nm 7.0×10^{9}@1000 nm	0.0	Heptamethine Salts	[11]
	Perovskite	300-800	2.7×10^{12}@650 nm	0.0		[12]

	Active material	Wavelength range (nm)	D^* (Jones)	Bias (V)	Comment	Ref.
Narrowband	P3HT:NT812: Y6	860	1.2×10^{13}@860 nm	-0.1	EDN	[13]
	P3HT:PTB7 :$PC_{71}BM$	745	1.1×10^{12}@745 nm	0.0		[14]
	DCV5T-Me: C_{60}	400-700	1.8×10^{12}@590 nm	0.0	CT absorption/ Small molecule	[15]
	PBTTT: $PC_{61}BM$	700-1700	5.0×10^{12}@800 nm 1.0×10^{13}@960 nm	0.0	CT absorption /Polymer	[16]
	ZnPc:C_{60}	810-1550	1.0×10^{11} (upper limit)	0.0	CT absorption/ Small molecule	[17]
	P3HT: $PC_{71}BM$	650	1.3×10^{11}@650 nm	-10.0	PM	[18]
	PCDTBT: $PC_{70}BM$	680	1.7×10^{12}@680 nm	-1.0	CCN	[19]
	Perovskite	650	1.9×10^{11}@650 nm	-0.5	CCN	[20]
	This work	**400-1100**	**2.4×10^{14}@495 nm** **2.8×10^{14}@550 nm** **3.0×10^{14}@615 nm** **2.5×10^{14}@660 nm** **1.0×10^{14}@724 nm** **1.1×10^{14}@754 nm** **1.3×10^{14}@790 nm** **1.1×10^{14}@810 nm** **7.7×10^{13}@840 nm** **4.2×10^{11}@905 nm** **4.2×10^{11}@950 nm** **3.2×10^{11}@1000 nm** **2.2×10^{11}@1035 nm**	**0.0**	**Transmission cavity**	

Supporting References

[1] W. Jang, S. Rasool, B. G. Kim, J. Kim, J. Yoon, S. Manzhos, H. K. Lee, I. Jeon, D. H. Wang, *Adv. Funct. Mater.* **2020**, 30, 2001402.

[2] G. H. Liu, T. F. Li, X. W. Zhan, H. B. Wu, Y. Cao, *ACS Appl. Mater. Interfaces* **2020**, 12, 17781.

[3] C. C. Lee, R. Estrada, Y. Z. Li, S. Biring, N. R. A. Al Amin, M. Z. Li, S. W. Liu, K. T. Wong, *Adv. Opt. Mater.* **2020**, 8, 2000519.

[4] W. Li, Y. L. Xu, X. Y. Meng, Z. Xiao, R. M. Li, L. Jiang, L. H. Cui, M. J. Zheng, C. Liu, L. M. Ding, Q. Q. Lin, *Adv. Funct. Mater.* **2019**, 29, 1808948.

[5] Z.-X. Liu, T.-K. Lau, G. Zhou, S. Li, J. Ren, S. K. Das, R. Xia, G. Wu, H. Zhu, X. Lu, *Nano Energy* **2019**, 63, 103807.

[6] V. Yeddu, G. Seo, F. Cruciani, P. M. Beaujuge, D. Y. Kim, *ACS Photonics* **2019**, 6, 2368.

[7] X. F. Xu, X. B. Zhou, K. Zhou, Y. X. Xia, W. Ma, O. Inganas, *Adv. Funct. Mater.* **2018**, 28, 1805570.

[8] Y. Z. Wei, Z. W. Ren, A. D. Zhang, P. Mao, H. Li, X. H. Zhong, W. W. Li, S. Y. Yang, J. Z. Wang, *Adv. Funct. Mater.* **2018**, 28, 1706690.

[9] J. Han, J. Qi, X. Zheng, Y. Wang, L. Hu, C. Guo, Y. Wang, Y. Li, D. Ma, W. Qiao, *J. Mater. Chem. C* **2017**, 5, 159.

[10] C. Liu, H. Peng, K. Wang, C. Wei, Z. Wang, X. Gong, *Nano Energy* **2016**, 30, 27.

[11] M. Young, J. Suddard-Bangsund, T. J. Patrick, N. Pajares, C. J. Traverse, M. C. Barr, S. Y. Lunt, R. R. Lunt, *Adv. Opt. Mater.* **2016**, 4, 1028.

[12] Q. Lin, A. Armin, D. M. Lyons, P. L. Burn, P. Meredith, *Adv. Mater.* **2015**, 27, 2060.

[13] B. Xie, R. Xie, K. Zhang, Q. Yin, Z. Hu, G. Yu, F. Huang, Y. Cao, *Nat. Commun.* **2020**, 11, 1.

[14] S. Xing, X. Wang, E. Guo, H. Kleemann, K. Leo, *ACS Appl. Mater. Interfaces* **2020**, 12, 13061.

[15] J. Wang, S. Ullbrich, J.-L. Hou, D. Spoltore, Q. Wang, Z. Ma, Z. Tang, K. Vandewal, *ACS*

Photonics **2019**, 6, 1393.

[16] Z. Tang, Z. Ma, A. Sanchez-Diaz, S. Ullbrich, Y. Liu, B. Siegmund, A. Mischok, K. Leo, M. Campoy-Quiles, W. Li, K. Vandewal, *Adv. Mater.* **2017**, 29, 1702184.

[17] B. Siegmund, A. Mischok, J. Benduhn, O. Zeika, S. Ullbrich, F. Nehm, M. Bohm, D. Spoltore, H. Frob, C. Korner, K. Leo, K. Vandewal, *Nat. Commun.* **2017**, 8, 15421.

[18] W. Wang, F. Zhang, M. Du, L. Li, M. Zhang, K. Wang, Y. Wang, B. Hu, Y. Fang, J. Huang, *Nano Lett.* **2017**, 17, 1995.

[19] A. Armin, R. D. Jansen-van Vuuren, N. Kopidakis, P. L. Burn, P. Meredith, *Nat. Commun.* **2015**, 6, 6343.

[20] Q. Lin, A. Armin, P. L. Burn, P. Meredith, *Nat. Photonics* **2015**, 9, 687.